

1 **The cold ion population at geosynchronous orbit and transport to the dayside**
2 **magnetopause: September 2015 to February 2016.**

3
4 *M. H. Denton^{1,2}, M. G. Henderson³, N. Maruyama^{4,5}, and S. A. Fuselier^{6, 7}.*

5
6 1. Center for Space Plasma Physics, Space Science Institute, CO 80301, USA.

7 2. New Mexico Consortium, Los Alamos, NM 87544, USA.

8 3. ISR-1, Los Alamos National Laboratory, NM 87545, USA.

9 4. Cooperative Institute for Research in Environmental Sciences, University of Colorado, Boulder,
10 Colorado, 80305, USA.

11 5. Space Weather Prediction Center, National Oceanic and Atmospheric Administration, Boulder,
12 Colorado, 80305, USA.

13 6. Southwest Research Institute (SwRI), San Antonio, TX 78238, USA.

14 7. University of Texas at San Antonio, San Antonio, TX 78249, USA

15

ABSTRACT

16
17
18
19
20
21
22
23
24
25
26
27
28
29
30

During intervals of enhanced magnetospheric convection, a high-density plume of cold ions is eroded from the plasmasphere and can flow toward the dayside magnetopause where it has the potential to reduce the rate of magnetic reconnection. In any interval of long-duration enhanced convection, tons of ions may follow such a trajectory. The study here concerns cold ion observations from geosynchronous orbit (GEO) during both calm and active periods. Probability distributions of the cold ion density and cold ion flow speed are determined during the six-month period from September 2015 to February 2016, inclusive. During low geomagnetic activity the cold, dense ions are in co-rotation with the Earth and flow speeds rarely exceed 10 km s^{-1} . During elevated geomagnetic activity, the cold ions between 12-18 MLT are observed to flow towards the dayside magnetosphere with a speed $>10 \text{ km s}^{-1}$ ~50% of the time. The *Shue et al.* [1998] model of the magnetopause location is used to derive the distribution of approximate *minimum* times for the cold ions to be transported from GEO to the dayside magnetopause. On average, during enhanced convection periods ($K_p > 3$) ions will take a mean time of ~4.5 hours to travel from GEO to the dayside magnetopause.

31 **1. Introduction**

32 Cold ions (<1 eV to ~tens eV) in the Earth's plasmasphere are the primary constituent contributing to
33 the mass density in the Earth's magnetosphere with a total mass $\sim 10^2$ - 10^3 metric tons [*Borovsky and*
34 *Denton, 2008; Goldstein et al., 2018*]. These ions are predominately H^+ , but there is a relatively large
35 concentration of He^+ in the plasmasphere. Previous work has revealed the importance of this
36 population in terms of its role in: (i) mass-loading of the dayside reconnection site [*Borovsky and*
37 *Denton, 2006, 2008; Walsh et al., 2013; Borovsky et al., 2013; Fuselier et al., 2017, 2018*];
38 contributing to wave-growth and wave-particle interactions in general [*MacDonald et al., 2008, 2010;*
39 *Posch et al., 2010; Blum et al., 2012; Borovsky et al., 2014*]; refilling of the plasmasphere and warm
40 plasma cloak following intervals of enhanced magnetospheric convection [*Chappell et al., 1971;*
41 *Carpenter and Lemaire, 1997; Su et al., 2001; Denton and Borovsky, 2014*]; and (iv) the total inertia in
42 the magnetospheric system [*Denton et al., 2014; Goldstein et al., 2018*].

43

44 During times of enhanced convection the dense cold ions co-rotating in the Earth's plasmasphere can
45 transition to drift paths that transport the plasma to the dayside reconnection site in the form of a
46 plasmaspheric drainage plume (e.g. *Borovsky and Denton [2006]; Darrouzet et al. [2008]; Walsh et al.*
47 *[2013]; Cassak and Fuselier [2016]*). At the reconnection site itself, the plasma can directly modulate
48 the rate of magnetic reconnection [*Borovsky and Denton, 2006; Cassak and Shay, 2007; Borovsky,*
49 *2013; Birn et al., 2008; Walsh et al., 2014a; 2014b; Cassak and Fuselier, 2016; Fuselier et al., 2017*].

50 Other physical effects of cold ions at the dayside magnetopause have also been investigated including
51 modification of Hall physics by the cold ions [*André et al., 2016*] and cold ion demagnetization near
52 the reconnection site [*Toledo-Redondo et al., 2016*]. During long-duration enhanced-convection
53 events (e.g. high-speed solar-wind streams) a total mass of ~tens of tons of ions can flow to the dayside

54 [Borovsky and Denton, 2008].

55

56 Geosynchronous orbit (GEO) at 6.6 Earth radii (R_E) is an ideal location at which to survey the plasma
57 transitioning from the co-rotating plasmasphere towards the dayside reconnection site. At this distance
58 from the Earth, orbiting satellites co-rotate with the Earth and suitable instrumentation can measure the
59 in-situ plasma as it also co-rotates, or as it moves radially outwards towards the dayside during periods
60 of enhanced convection in a plasmaspheric drainage plume [Borovsky and Denton; 2006; 2008]. Los
61 Alamos National Laboratory (LANL) satellites orbiting at GEO have the necessary instrumentation to
62 sample the cold (and hot) plasma [Bame et al., 1993; Thomsen et al., 1999] and have been used in
63 numerous studies to determine the characteristics of this plasma under a range of different conditions
64 (e.g. Denton et al. [2005;2017]; Borovsky and Denton [2006; 2008]; Denton and Borovsky [2008;
65 2014]).

66

67 The primary objective of the current study is to survey cold ions during the interval September 2015 to
68 February 2016 (inclusive). These specific dates are chosen since during this period the four satellites
69 that form the Magnetosphere MultiScale (MMS) mission [Fuselier et al., 2016] are orbiting close to
70 the dayside magnetopause and sample cold plasma [Young et al., 2014] that has been delivered to the
71 region during periods of enhanced convection. These measurements include ion composition, wave
72 measurements of the total plasma density, and, at times, active reduction of the spacecraft potential in
73 order to better observe the low-energy ions. During the same period, the twin Van Allen Probes
74 satellites are orbiting in the inner magnetosphere inwards of GEO and also provide cold ion
75 measurements including the ion composition [Funsten et al., 2013], the erosion flux [Foster et al.,
76 2014], and electromagnetic wave properties of the plasma. Thus, there is the potential for three

77 independent data-sets to provide a capability to track cold ions as they transition from the inner
78 magnetosphere, via GEO, out towards the dayside reconnection site. There are >100 conjunctions of
79 the LANL, MMS, and Van Allen Probes satellites in this period (with a conjunction being defined as
80 one satellite from each constellation being aligned on the dayside radially outwards from inner
81 magnetosphere to magnetopause). In this current study the probability distribution statistics of the cold
82 ions (density and flow-speed) between September 2015 and February 2016 are determined as a
83 function of geomagnetic activity at GEO. Using these probability distributions, combined with a
84 model of the magnetopause stand-off distance [*Shue et al.*, 1998], allows the distribution of cold-ion
85 transport times from GEO to the magnetopause to be estimated in a statistical manner. Such analyses
86 of the statistical distribution of the cold ions at GEO are intended to enable follow-on studies that
87 compare and contrast the statistics of the cold plasma observed by LANL satellites at GEO with the
88 same plasma observed in the inner magnetosphere with Van Allen Probes and at the dayside
89 magnetopause with MMS.

90

91 **2. Data**

92 The main data set used in the current study is that provided from LANL satellites orbiting at GEO.
93 The Magnetospheric Plasma Analyzer (MPA) instruments onboard LANL satellites sample the plasma
94 (electrons and ions) at GEO in the energy range ~1 eV to ~40 keV. MPA is a spherical sector electro-
95 static analyzer comprising six detectors measuring forty logarithmically-spaced energy channels.
96 Situated on a spinning spacecraft MPA is able to provide full three-dimensional particle distributions
97 for the ions and electrons once every 86 seconds. A full description of the instrument and the analysis
98 software can be found in *Bame et al.* [1993] and *Thomsen et al.* [1999]. Since LANL spacecraft
99 usually charge in a negative sense, all positively charged ions are detected at all times by MPA. Two

100 particle populations can be present at GEO and the ion density and the ion velocity are calculated
101 directly from the moments of the distribution for both the cold (plasmasphere) and hot (plasma sheet)
102 populations [Thomsen *et al.*, 1999]. When calculating the moments, all ions are assumed to be protons.
103 Data from all available LANL satellites are used in the analysis in this study. Furthermore, LANL
104 satellites are located close to the geographic equator, with each orbiting at a slightly different
105 inclination. Effects due to orbital differences between satellites are not considered during this study
106 with all data assumed to originate from the geographic equator.

107

108 Figure 1 shows examples of MPA ion observations from a single satellite (01A) at GEO during calm
109 geomagnetic conditions ($K_p < 1$ with the plasmasphere in quasi-co-rotation with the Earth) and during
110 an interval of enhanced convection (plasma moving radially outwards from GEO towards the dayside)
111 (cf. Figure 12 of Borovsky and Denton [2008]). The number density of the magnetospheric ions is
112 indicated by the color bar and the line vectors indicate the flow direction in the geographic xy-plane as
113 a function of magnetic local time (MLT) and position. Here, MLT is calculated as follows: firstly we
114 find the anti-sunward direction in geomagnetic coordinates (ϕ), secondly, we locate the spacecraft
115 longitudinal position (ϕ_{SC}) also in geomagnetic coordinates, and thirdly we define $MLT = UT + (\phi_{SC} -$
116 $\phi)/15$. Thus, here MLT is the coordinate that specifies the longitudinal location of the satellite around
117 geosynchronous orbit: local noon is the sub-solar point and local midnight is anti-sunward. For the 24
118 hour periods plotted, each 5th available data point is plotted for clarity. Additionally, to emphasize the
119 highest density plasma likely to have the greatest effect on the reconnection rate at the dayside, data
120 are only plotted if the plasma number density $> 10 \text{ cm}^{-3}$. The top panel shows data from a calm day in
121 2014. The high-density plasma during this day is in quasi-corotation with Earth (flow speed $\sim \text{few km s}^{-1}$)
122 ¹) i.e. the satellite is sampling the outer plasmasphere with no major sunward flows on the dayside. In

123 contrast, the bottom panel shows data from a disturbed day in 2015 when magnetospheric convection
124 was enhanced due to the passage of a high-speed solar-wind stream (HSS). There are substantial
125 sunward flows during this period ($>20 \text{ km s}^{-1}$) - the satellite is likely sampling plasma within a
126 drainage plume where plasma originally co-rotating in the Earth's plasmasphere is now transported to
127 the dayside due to the enhanced convection. The plasma flowing towards the dayside magnetopause is
128 the main subject of interest in this study.

129

130 **3. Analysis and Results**

131

132 **3.1 The cold ion distribution at GEO**

133 Analysis of the LANL/MPA data is carried out in order to reveal the characteristic density and flow-
134 speed of the plasma at GEO and the plasma that is transported towards the dayside. However, the cold
135 ion flux at a particular energy is also variable. As a first step, the mean ion flux at two energies is
136 calculated for all available observations from the LANL/MPA data set in the period 1990 to 2008.
137 This period is chosen since it is the same period used in many previous statistical studies concerning
138 the cold ion population (e.g. *Borovsky and Denton* [2008, 2009, 2010]; *Denton and Borovsky* [2008,
139 2009, 2012]). In the current study data are binned into one of 24 magnetic local time bins, and one of
140 28 discrete bins based on the Kp index [*Bartels et al.*, 1939]. The Kp index correlates very well with
141 large-scale magnetospheric convection [*Thomsen*, 2004]. Magnetosheath intervals are filtered out of
142 the analysis. The mean ion flux in each bin is then calculated at $\sim 11 \text{ eV}$ and $\sim 1 \text{ keV}$ and plotted in
143 Figure 2. There are over 10 million unique data points contributing to each panel in Figure 2 and this
144 figure very clearly highlights the different statistical behaviour of ions sampled at GEO based on their
145 energy. Low energy ions (top panel) with energies of a few eV are part of the plasmasphere and

146 plasmaspheric drainage plume population. This population is detected at all magnetic local times
147 during low activity (plasmasphere - $K_p < \sim 2$). During enhanced convection ($K_p > \sim 2$) the outer
148 regions of the plasmasphere are transported to the dayside magnetosphere in the form of a
149 plasmasphere drainage plume that is clearly visible as the elevated fluxes in the noon to dusk sector
150 (~ 12 - 18 MLT). The flux peak is shifted from ~ 18 MLT toward 12 MLT and the peak flux tends to
151 decrease slightly as K_p increases.

152

153 Higher energy ions (bottom panel) with energies of a few keV are part of the ion plasma sheet
154 population. The measured flux of these ions is enhanced during elevated convection intervals as new
155 dense plasma enters the inner magnetosphere from the magnetotail. Previous work has clearly
156 demonstrated that the different drift paths that each population follows, and the general behaviour of
157 each population, are largely determined by the particle energy [*Korth et al.*, 1999; *Fernandes et al.*,
158 2017] and lead to the enhancement in ion flux observed for very high K_p values. While there are
159 occasions where both populations low-energy and high-energy ions are observed in the same spatial
160 location by MPA, it is clear from Figure 2 that statistically the two populations do not overlap to any
161 significant degree - the two populations (hot and cold) are following different drift paths. Recent
162 work by *Denton et al.* [2016] does explore one occasion when high-energy and low-energy plasma are
163 co-located. That study demonstrated that low energy ions don't necessarily originate directly from the
164 outer regions of the plasmasphere in the form of a plasmaspheric drainage plume in the post-noon
165 sector. An alternative transport path, from the nightside region, carries low energy ions towards the
166 dayside reconnection site via the dawn sector, rather than from dusk. Such ions arrive on the dayside
167 and abut the plasmaspheric drainage plume, although they have taken very different drift paths to
168 arrive there (see Figure 4 and Supp. Mat. of *Denton et al.* [2016]). However, the main population of

169 interest in the current study is low energy ions that form the plasmasphere and drainage plume (top
170 panel).

171

172 **3.2 Cold ions and their variation with activity**

173 The period of interest in the current study is the six-month interval from September 2015 to February
174 2016 (when >100 conjunctions with the MMS spacecraft orbiting near the dayside magnetopause
175 occur). For this period all data are analyzed for all conditions (active and calm), as a function of
176 magnetic local time and activity proxied by the Kp index.

177

178 Figure 3 contains scatter plots of all cold ion number density (N) and xy-flow speed (V) observations
179 made by MPA, and plotted here as a function of magnetic local time and the Kp index (again,
180 magnetosheath intervals are filtered out). As can be seen in the top panel of the figure, the cold ions
181 are to be found at all magnetic local times around GEO, with a typical number density $>1 \text{ cm}^{-3}$. The
182 highest densities observed are $>100 \text{ cm}^{-3}$ and occur in the post-noon sector (12-18 MLT) where the
183 plasmaspheric drainage plume is typically located during enhanced convection intervals. As found in
184 previous studies, the density and the flow-speed of the plume (and the plume density structure itself)
185 are correlated with Kp, and with the age of each plume [cf. Figures 10 and 11 of *Borovsky and Denton,*
186 2008], although it should be noted that geomagnetic activity during the six-month period under study
187 here was quite low with less frequent intervals of $Kp > 3$ than those used in the previous work
188 referenced above. The mean Kp for the period under investigation is $\sim 2^+$.

189

190 The bottom panel of Figure 3 shows the flow speed in the spacecraft xy (geographic) plane (see
191 *Thomsen et al.* [1999]). A flow speed greater than $\sim 10 \text{ km s}^{-1}$ indicates a large deviation from co-

192 rotation and in the post-noon region where a plasmaspheric plume is expected, the dense cold ions are
193 generally moving rapidly to the dayside magnetopause with the flow speed in this region being well-
194 correlated with Kp - the highest speeds are typically observed during elevated Kp intervals, again in
195 line with previous observations (e.g. Figure 3 of *Denton and Borovsky* [2012]).

196

197 In order to quantify the probability distributions of the density and velocity of the cold ions during
198 quiet and disturbed intervals, we calculate the probability distributions for all data plotted in Figure 3,
199 but now separated into calm ($Kp < 1^+$) and disturbed ($Kp > 3$) intervals. The Kp cut-offs used in these
200 definitions were derived based on the expected statistical location of the plasmasphere and plume with
201 reference to Figure 2. Since we are particularly interested in ions that may be moving to the dayside
202 magnetopause (and thus the dayside reconnection site) we restrict the magnetic local times of the
203 observations to the post-noon sector values between 12 and 18 MLT. Figure 4 contains the probability
204 distributions for these calm and disturbed intervals for both N and V, along with statistical information
205 on each distribution. The left column in this figure shows the cold ion density and cold ion velocity for
206 $Kp < 1^+$. It is clear that during calm intervals, the cold ions are usually co-rotating with the Earth at
207 GEO with flow speeds $< 10 \text{ km s}^{-1}$, and have a typical density $\sim 10 \text{ cm}^{-3}$. The right column of the figure
208 shows the cold ion density and cold ion velocity for $Kp > 3$. During such active intervals the cold
209 plasma density is very slightly higher than during calm periods but in contrast, the flow speed of this
210 plasma is certainly greatly increased (cf. Figure 3). Given that speeds in excess of $\sim 10 \text{ km s}^{-1}$ indicate
211 a strong deviation from (quasi) co-rotation, and that the flow-vectors of this plasma are typically
212 directed sunwards (cf. Figure 1 and Figure 12 of *Borovsky and Denton*, 2008), it can be readily
213 concluded that this plasma is moving towards the dayside magnetopause. During the period studied
214 here, dayside directed flows at GEO exceed $\sim 10 \text{ km s}^{-1}$ roughly 50% of the time when $Kp > 3$.

215

216 **3.3 Cold ions transport times to the dayside magnetosphere**

217 The flow-speed of the ions is directly related to their transit time to the dayside magnetopause (and
218 hence to the dayside reconnection site). While more complex calculations are certainly possible, a
219 simple estimate of the *minimum* time taken for these ions to reach the dayside magnetopause from
220 GEO requires an estimate of how distant the magnetopause might be. This estimate is obtained: (i) by
221 utilizing the *Shue et al.* [1998] model for magnetopause standoff distance, (ii) by assuming the flow is
222 directed from GEO in a straight line to the dayside magnetopause, and (iii) by assuming the speed of
223 the plasma measured at GEO remains constant from GEO to this location. Hence, while more
224 sophisticated estimates of the ion transport time can be carried out in future (particularly for individual
225 spacecraft conjunction studies), the results of the current analysis provide a valuable estimate of the
226 *minimum* transport time from GEO to the magnetopause.

227

228 Figure 5 contains the probability distribution for the transport time (in hours) from GEO to the
229 estimated magnetopause location for the same data as is plotted in the right column of Figure 4 ($K_p > 3$,
230 12-18 MLT). Each transport time contributing to this distribution is calculated based on the
231 instantaneous solar wind conditions that drive the *Shue et al.* [1998] model, and on the instantaneous
232 flow-speed at GEO. Such analysis relates the plasma characteristics at GEO with those that may be
233 subsequently detected at the dayside reconnection site (e.g. by MMS satellites). It is clear from Figure
234 5 that transit times of a few hours are typical, with a mean transport time of ~ 4.5 hours for ions
235 arriving at the magnetopause from GEO

236

237 **4. Discussion**

238 The effects of cold ions on the rate of magnetic reconnection at the dayside magnetopause are still
239 being evaluated. Our current understanding is that the dayside reconnection rate is likely to be reduced
240 in the presence of dense, cold ions at the magnetopause, since these ions create conditions that favor
241 asymmetric reconnection [Cassak and Shay, 2007; Birn et al., 2008]. Borovsky and Denton [2008]
242 calculated that tons of ions (protons) were likely being transported to the dayside magnetopause during
243 long-duration enhanced convection conditions such as those found during HSSs. Should there be a
244 substantial presence of heavy ions then the total mass density of ions will be greater still. Borovsky
245 and Denton [2008] also provided estimates of correction factors to be applied to the observations in the
246 case of a plasma with substantial heavy ion composition. For a plasma with 70% H⁺, 20% He⁺ and
247 10% O⁺ then the total overall density would be multiplied by 1.21. At a reconnection site, a higher
248 mass density on the magnetospheric side would certainly cause changes in the rate of magnetic
249 reconnection, potentially reducing the reconnection rate still further [Cassak and Shay, 2007; Birn et
250 al., 2008].

251
252 Observational studies have provided statistical and case-study evidence for a reduction in the
253 reconnection rate due to the presence of dense, cold ions at the dayside magnetopause [Borovsky and
254 Denton, 2006; McPhadden et al., 2008; Borovsky et al., 2013; Walsh et al., 2013; 2014a; 2014b;
255 Fuselier et al., 2017]. However, there is a debate as to whether the local or global reconnection rate is
256 affected. Borovsky and Birn [2014] argue that the local conditions at the reconnection site (by
257 necessity including the cold ion density) control the magnetic reconnection rate at the dayside
258 magnetopause. In contrast, Lopez [2016] suggests that the solar wind itself is the primary factor
259 controlling the total integrated reconnection rate on the dayside, and that localized density changes on
260 the magnetospheric side of the reconnection site merely affect the local reconnection rate, rather than

261 the integrated total.

262

263 This study is a first step in more-fully determining the role of cold ions affecting the rate of magnetic
264 reconnection at the dayside, in both a local and global sense. We have quantified the flow-speed and
265 density of the ions transported towards the dayside from GEO during enhanced convection and
266 provided estimates of the timescales for such transport to occur over. These values are intended to
267 provide modelers with quantitative estimates of how much cold plasma is moving to the dayside via
268 GEO and the timescales such transport occurs over. Future work will couple the full capabilities of the
269 Van Allen Probes satellites in the inner magnetosphere, the LANL satellites at GEO, and the MMS
270 satellites near the dayside reconnection site to provide a detailed description of: (a) the low-energy ion
271 transport to the dayside, (b) the electro-magnetic wave characteristics within the plasma, (c) the
272 potential evolution of the ions due to wave-particle interactions occurring as they drift, (d) the
273 composition of the ions and the total mass density that travels from the inner magnetosphere to the
274 dayside magnetopause, and (e) the subsequent role of the low-energy ions in modulating the rate of
275 dayside magnetic reconnection.

276

277 **5. Summary**

278

279 1. Cold ion data from LANL/MPA satellites are analyzed during the interval September 2015 to
280 February 2016 in order to understand the characteristics of plasma that is transported to the dayside
281 magnetopause from GEO. Probability distributions of the cold ion flow speed and cold ion density
282 during this period are determined. These indicate densities of $\sim 10 \text{ cm}^{-3}$ and flow speeds in excess of
283 10 km s^{-1} during enhanced convection ($K_p > 3$) compared to calm intervals ($K_p < 1^+$).

284

285 2. Plasma flows are directed to the dayside magnetopause ~50% of the time for $K_p > 3$. Plasma is in
286 quasi-corotation during intervals when $K_p < 1^+$.

287

288 3. The distribution of expected *minimum* transport times for the ion plasma from GEO to the
289 magnetopause indicates that ions arrive at the dayside magnetopause within a few hours (mean
290 transport time ~4.5 hours). Such quantification of cold ion flows enable estimates of the effect of cold
291 ions on dayside reconnection to be made in future studies.

292

293 **Acknowledgements**

294 The authors acknowledge the OMNI database for the solar wind and geophysical parameters used in
295 this study. This work was primarily supported by the NASA Living With A Star (LWS) grant
296 NNX16AB83G, as well as NASA grant NNX16AB75G, NASA LWS Grant: 80NSSC17K0682 and
297 NASA H-SR grant 80NSSC19K1107 . MHD thanks Joe Borovsky and Lauren Blum for many useful
298 discussions. .Data used in the study are available in the Zenodo repository.

299 **References**

300

301 André, M., et al. (2016), Magnetic reconnection and modification of the Hall physics due to cold ions
302 at the magnetopause, *Geophys. Res. Lett.*, 43, 6705–6712, doi:10.1002/2016GL069665.

303

304 Bame, S. J., D. J. McComas, M. F. Thomsen, B. L. Barraclough, R. C. Elphic, J. P. Glore, J. C.
305 Chavez, E. P. Evans and F. J. Wymer, *Rev. Sci. Instrum.*, 64, 1026-1033, 1993.

306

307 Bartels, J., N. A. H. Heck, and H. F. Johnstone, The three-hour-range index measuring geomagnetic
308 activity, *J. Geophys. Res.*, 44, 411-454, 1939.

309

310 Birn, J., J. E. Borovsky, and M. Hesse, Properties of asymmetric magnetic reconnection, *Phys.*
311 *Plasmas*, 15, 032101, doi:10.1063/1.2888491, 2008.

312

313 Blum, L. W., E. A. MacDonald, L. B. N. Clausen, and X. Li (2012), A comparison of magnetic field
314 measurements and a plasma-based proxy to infer EMIC wave distributions at geosynchronous
315 orbit, *J. Geophys. Res.*, 117, A05220, doi:10.1029/2011JA017474.

316

317 Borovsky, J. E., and M. H. Denton, The effect of plasmaspheric drainage plumes on solar-
318 wind/magnetosphere coupling, *Geophys. Res. Lett.*, 33, L20101, 2006.

319

320 Borovsky, J. E., and M. H. Denton, A statistical look at plasmaspheric drainage plumes, *J. Geophys.*
321 *Res.*, 113, A09221, 2008.

322

323 Borovsky, J. E., and M. H. Denton, Electron loss rates from the outer electron radiation belt caused by
324 the filling of the outer plasmasphere: The calm before the storm, *J. Geophys. Res.*, 114, A11203,
325 doi:10.1029/2009JA014063, 2009.

326

327 Borovsky, J. E., D. T. Welling, M. F. Thomsen, and M. H. Denton (2014), Long-lived plasmaspheric
328 drainage plumes: Where does the plasma come from? *J. Geophys. Res. Space Physics*, 119,
329 doi:10.1002/2014JA020228.

330

331 Borovsky, J. E., M. H. Denton, R. E. Denton, V. K. Jordanova, and J. Krall, Estimating the effects of
332 ionospheric plasma on solar-wind/magnetosphere coupling via mass loading of dayside
333 reconnection: Ion-plasma-sheet oxygen, plasmaspheric drainage plumes, and the plasma cloak, *J.*
334 *Geophys. Res. Space Physics*, 118, 5695–5719, 2013.

335

336 Borovsky, J. E., Physical improvements to the solar wind reconnection control function for the Earth's
337 magnetosphere, *J. Geophys. Res. Space Physics*, 118, 2113–2121, 2013.

338

339 Borovsky, J. E., R. H. W. Friedel, and M. H. Denton, Statistically Measuring the Amount of Pitch-
340 Angle Scattering that Energetic Electrons Undergo as they Drift across the Plasmaspheric
341 Drainage Plume at Geosynchronous Orbit, *J. Geophys. Res.*, doi:10.1002/2013JA019310, 2014.

342

343 Carpenter, D. L., and J. Lemaire, Erosion and recovery of the plasmasphere in the plasmopause region,
344 *Space Sci. Rev.*, 80, 153, 1997.

345

346 Cassak P. A., and M. A. Shay, Scaling of asymmetric magnetic reconnection: General theory and
347 collisional simulations, *Phys. Plasmas*, 14, 102114, doi:1070-664X/2007/14(10)/102114/11, 2007.

348

349 Cassak, P. A., and S. A. Fuselier, Reconnection at Earth's dayside magnetopause, in *Magnetic*
350 *Reconnection*, edited by W. Gonzalez and E. Parker, *Astrophys. and Space Sci Library*, 427,
351 Springer, Switzerland, doi:10.1007/978-3-319-26432-5, p. 213-276, 2016.

352

353 Chappell, C. R., K. K. Harris, and G. W. Sharp, OGO 5 measurements of the plasmasphere during
354 observations of stable auroral red arcs, *J. Geophys. Res.*, 76, 2357–2365, 1971.

355

356 Darrouzet, F., et al., Statistical analysis of plasmaspheric plumes with Cluster/WHISPER observations,
357 *Ann. Geophysicae.*, 26, 2403-2417, 2008.

358

359 Denton, M. H., and J. E. Borovsky (2008), Superposed epoch analysis of high-speed-stream effects at
360 geosynchronous orbit: Hot plasma, cold plasma, and the solar wind, *J. Geophys. Res.*, 113,
361 A07216, doi:10.1029/2007JA012998.

362

363 Denton, M. H., and J. E. Borovsky, The superdense plasma sheet in the magnetosphere during high-
364 speed-stream-driven storms: Plasma transport timescales. *J. Atmos. Sol-Terr. Phys*, 71, 1045-
365 1058, 2009

366

367 Denton, M. H., and J. E. Borovsky, Magnetosphere response to high-speed solar wind streams: A

368 comparison of weak and strong driving and the importance of extended periods of fast solar wind,
369 J. Geophys. Res., 117, A00L05, doi:10.1029/2011JA017124, 2012.

370

371 Denton, M. H., and J. E. Borovsky, Observations and modeling of magnetic flux tube refilling of the
372 plasmasphere at geosynchronous orbit, J. Geophys. Res. Space Physics, 119, 9246–9255, 2014.

373

374 Denton, M. H., and J. E. Borovsky, The response of the inner magnetosphere to the trailing edges of
375 high-speed solar-wind streams, J. Geophys. Res., 122, 501–516, doi:10.1002/2016JA023592,
376 2017.

377

378 Denton, M. H., M. F. Thomsen, H. Korth, S. Lynch, J. C. Zhang and M. W. Liemohn, Bulk plasma
379 properties at geosynchronous orbit, J. Geophys. Res., 110, A07223, 2005.

380

381 Denton, M. H., G. E. Reeves, M. F. Thomsen, M. G. Henderson, R. H. W. Friedel, B. Larsen, R. M.
382 Skoug, H. O. Funsten, H. E. Spence, C. A. Kletzing, The complex nature of storm-time ion
383 dynamics: Transport and local acceleration, Geophys. Res. Lett., 43, 1059-1067,
384 doi:10.1002/2016GL070878, 2016.

385

386 Denton, R. E., Takahashi, K., Thomsen, M. F., Borovsky, J. E., Singer, H. J., Wang, Y, Evolution of
387 mass density and O⁺ concentration at geostationary orbit during storm and quiet events. J.
388 Geophys. Res., 119, 6417–6431, 2014.

389

390 Fernandes, P. A., et al. (2017), The plasma environment inside geostationary orbit: A Van Allen

391 Probes HOPE survey, *J. Geophys. Res. Space Physics*, 122, doi:10.1002/2017JA024160.
392

393 Foster, J. C., Erickson, P. J., Coster, A. J., Thaller, S., Tao, J., Wygant, J. R., and Bonnell, J. W. (
394 2014), Storm time observations of plasmasphere erosion flux in the magnetosphere and
395 ionosphere, *Geophys. Res. Lett.*, 41, 762– 768, doi:10.1002/2013GL059124.
396

397 Funsten, H. O., R. M. Skoug, A. A. Guthrie, E. A. MacDonald, J. B. Baldonardo, R. W. Harper, K. C.
398 Henderson, K. H. Kihara, J. E. Lake, B. A. Larsen, A. D. Puckett, V. J. Vigil, R. H. Friedel, M. G.
399 Henderson, J. T. Niehof, G. D. Reeves, M. F. Thomsen, J. J. Hanley, D. E. George, J.-M. Jahn, S.
400 Cortinas, A. De Los Santos, G. Dunn, E. Edlund, M. Ferris, M. Freeman, M. Maple, C. Nunez, T.
401 Taylor, W. Toczynski, C. Urdiales, H. E. Spence, J. A. Cravens, L. L. Suther, and J. Chen,
402 Helium, Oxygen, Proton, and Electron (HOPE) mass spectrometer for the Radiation Belt Storm
403 Probes mission, *Space Sci. Rev.*, 179, 423-484, 2013.
404

405 Fuselier, S. A., W. S. Lewis, C. Schiff, R. Ergun, J. L. Burch, S. M. Petrinec, and K. J. Trattner,
406 Magnetospheric multiscale science emission profile and operations, *Space Sci. Rev.*, 199:77-103,
407 doi:10.1007/s11214-014-0087-x, 2016.
408

409 Fuselier S. A., et al. (2017), Magnetospheric ion influence at the dayside magnetopause, *J. Geophys.*
410 *Res. Space Physics*, 122, 8617-8631, doi:10.1002/2017JA024515.
411

412 Fuselier, S. A., et al. (2018), Observational evidence of large-scale multiple reconnection at the Earth's
413 dayside magnetopause, *J. Geophys. Res.*, 123, 8407-8421, <https://doi.org/10.1029/2018JA025681>.

414

415 Goldstein, J., Chappell, C. R., Davis, M. W., Denton, M. H., Denton, R. E., Gallagher, D. L., XXXX,

416 Imaging the global distribution of plasmaspheric oxygen. *J. Geophys. Res.*, 123, 2078–2103, 2018.

417

418 King, J. H., and N. E. Papitashvili, Solar wind spatial scales in and comparisons of hourly Wind and

419 ACE plasma and magnetic field data, *J. Geophys. Res.*, 110, A02104, 2005.

420

421 Korth, H., M. F. Thomsen, J. E. Borovsky, and D. J. McComas, Plasma sheet access to

422 geosynchronous orbit, *J. Geophys. Res.*, 104, 25,047 – 25,061, 1999.

423

424 Lopez, R. E. (2016), The integrated dayside merging rate is controlled primarily by the solar wind, *J.*

425 *Geophys. Res. Space Physics*, 121, 4435– 4445, doi:10.1002/2016JA022556.

426

427 MacDonald, E. A., M. H. Denton, M. F. Thomsen, and S. P. Gary, Superposed epoch analysis of a

428 whistler instability criterion at geosynchronous orbit during geomagnetic storms, *J. Atmos. Sol-*

429 *Terr. Phys.* 70, 1789-1796, 2008.

430

431 MacDonald, E. A., L. W. Blum, S. P. Gary, M. F. Thomsen, and M. H. Denton, High-speed stream

432 driven inferences of global wave distributions at geosynchronous orbit; relevance to radiation belt

433 dynamics, *Proc. Roy. Soc. A.*, 466, 3351-3362, 2010.

434

435 McFadden, J. P., C. W. Carlson, D. Larson, J. Bonnell, F. S. Mozer, V. Angelopoulos, K.-H.

436 Glassmeier, and U. Auster, Structure of plasmaspheric plumes and their participation in

437 magnetopause reconnection, First results from THEMIS, *Geophys. Res. Lett.*, 35, L17S10,
438 doi:10.1029/2008GL033677, 2008.

439

440 Posch, J. L., M. J. Engebretson, M. T. Murphy, M. H. Denton, M. R. Lessard, and R. B. Horne,
441 Probing the relationship between EMIC waves and plasmaspheric plumes near geosynchronous
442 orbit, *J. Geophys. Res.*, 115, A11205, 2010.

443

444 Shue, J.H., et al., Magnetopause location under extreme solar wind conditions, *J. Geophys. Res.*, 103(
445 A8), 17691– 17700, doi:10.1029/98JA01103, 1998.

446

447 Su, Y.-J., M. F. Thomsen, J. E. Borovsky, and D. J. Lawrence, A comprehensive survey of
448 plasmasphere refilling at geosynchronous orbit, *J. Geophys. Res.*, 106, 25,615–25,629, 2001.

449

450 Thomsen, M. F., Why Kp is such a good measure of magnetospheric convection, *Space Weather*, 2,
451 S11004, doi:10.1029/2004SW000089, 2004.

452

453 Thomsen, M. F., E. Noveroske, J. E. Borovsky, and D. J. McComas, Calculating the Moments from
454 Measurements by the Los Alamos Magnetospheric Plasma Analyzer, LA-13566-MS, Los Alamos
455 National Laboratory, 1999.

456

457 Toledo-Redondo, S., et al. (2016), Cold ion demagnetization near the X-line of magnetic reconnection,
458 *Geophys. Res. Lett.*, 43, 6759–6767, doi:10.1002/2016GL069877.

459

460 Walsh, B. M., D. G. Sibeck, Y. Nishimura, and V. Angelopoulos (2013), Statistical analysis of the
461 plasmaspheric plume at the magnetopause, *J. Geophys. Res. Space Physics*, 118, 4844–4851,
462 doi:10.1002/jgra.50458.

463

464 Walsh, B. M., et al., The plasmaspheric plume and magnetopause reconnection, *Geophys. Res. Lett.*,
465 10.1002/2013GL058802, 2014a.

466

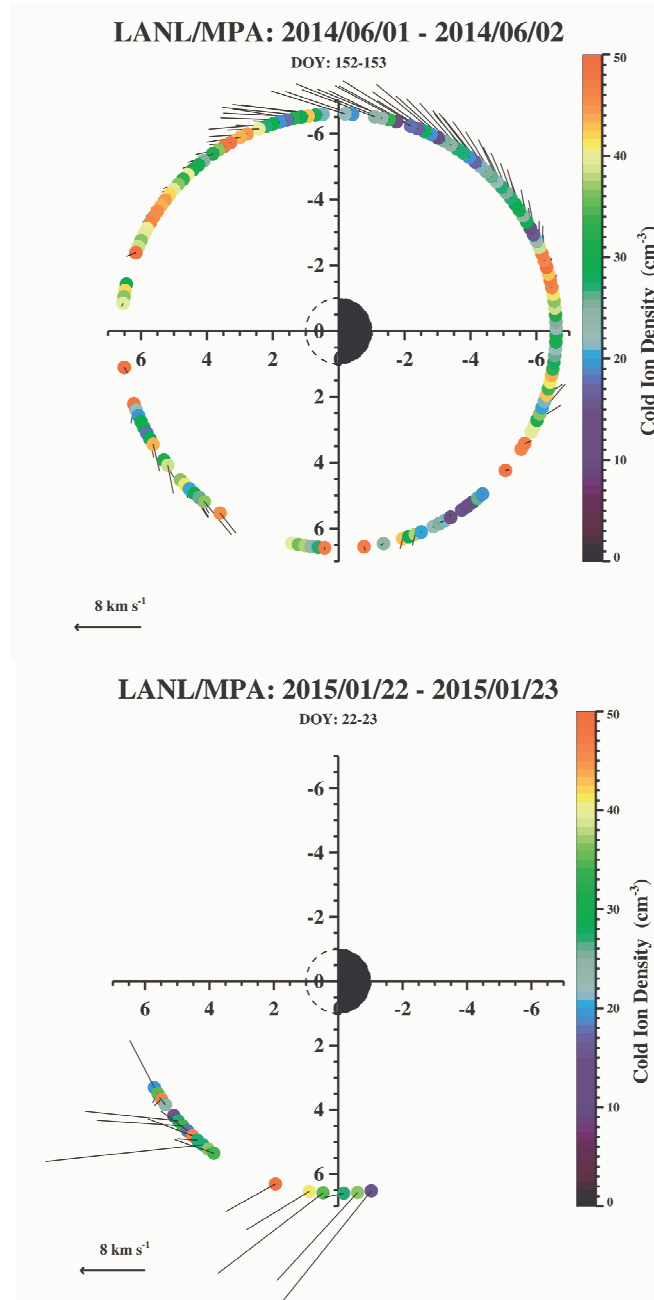
467 Walsh, B. M., et al., Simultaneous Ground- and space-based observations of the plasmaspheric plume
468 and reconnection, *Science*, 343, 1122, 2014b.

469

470 Young, D. T., et al., Hot plasma composition analyzer for the magnetospheric multiscale mission,
471 *Space Sci. Rev.*, doi:10.1007/s11214-014-0049-6, 2014.

472

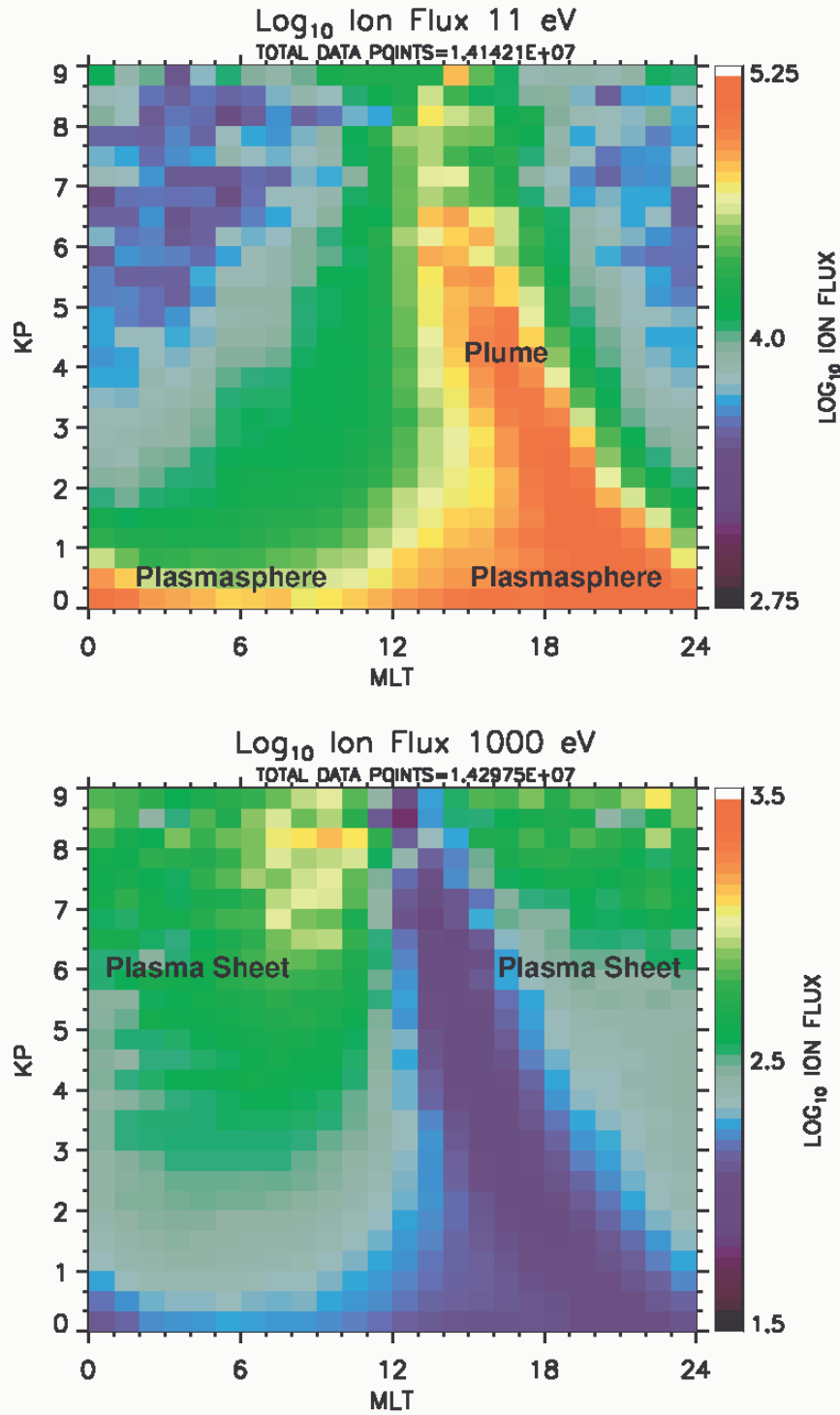
473
474



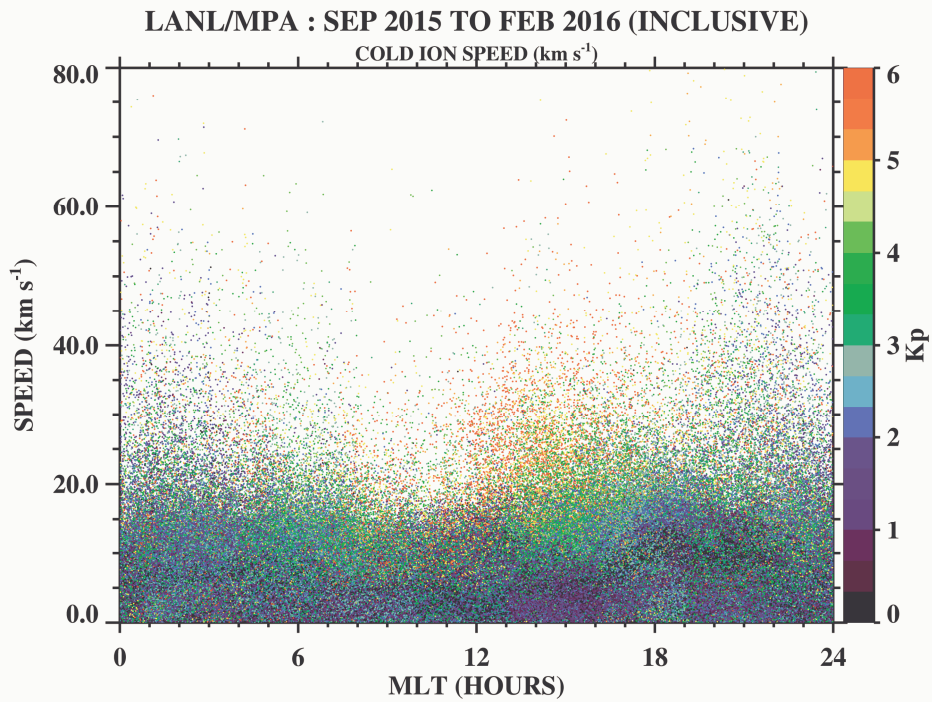
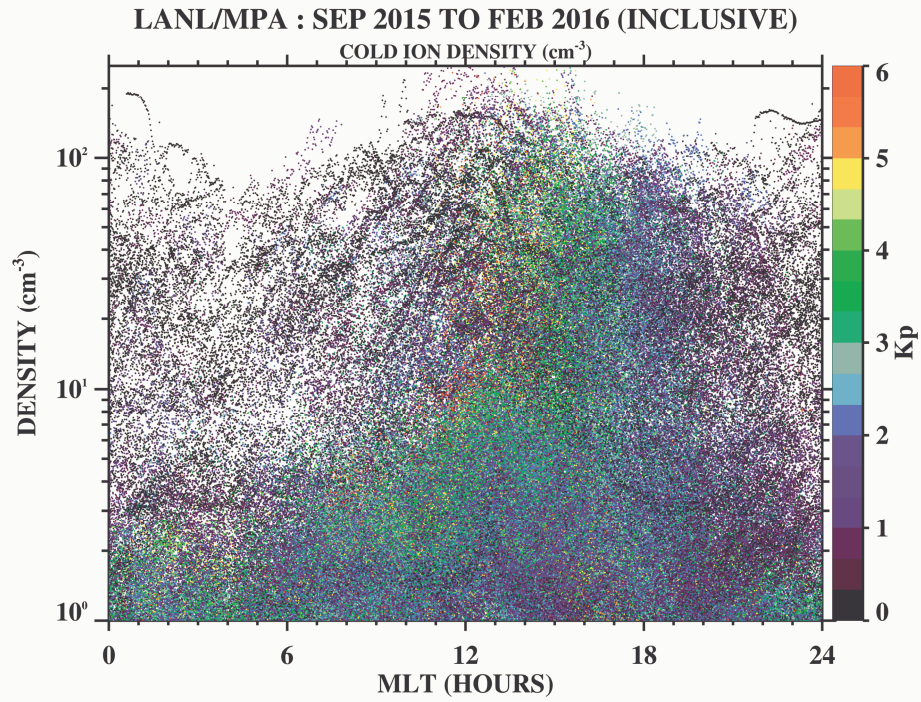
475

476
477

478 **Figure 1.** Example ion density and flow vectors measured by a single LANL satellite (01A) during a
479 calm period in 2014 when co-rotation dominates (top) and a disturbed period in 2015 when flow to the
480 dayside occurs (bottom).



481
 482 **Figure 2.** The mean ion flux calculated from MPA observations at GEO at two energies, and as a
 483 function of magnetic local time and the Kp index (1990-2008 inclusive). The low energy ions (top
 484 panel) comprise the plasmasphere and drainage plume population (few eV) whereas the higher energy
 485 ions (~ keV) are the population of plasma sheet. All ions are assumed to be protons. It is clear that
 486 these two populations vary significantly with Kp, but do not generally overlap as they are typically on
 487 different drift trajectories.



488

489

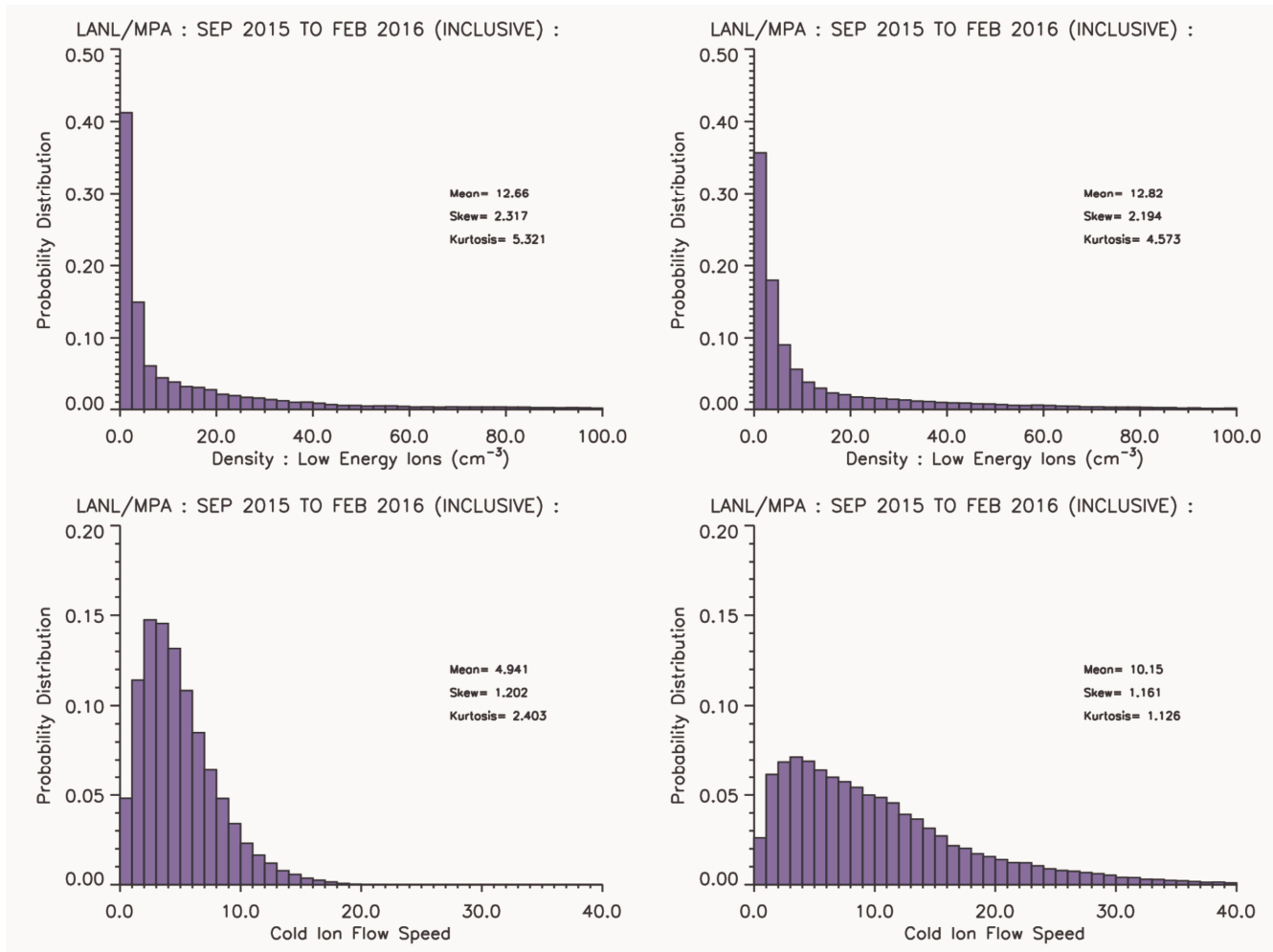
490

491

492

493

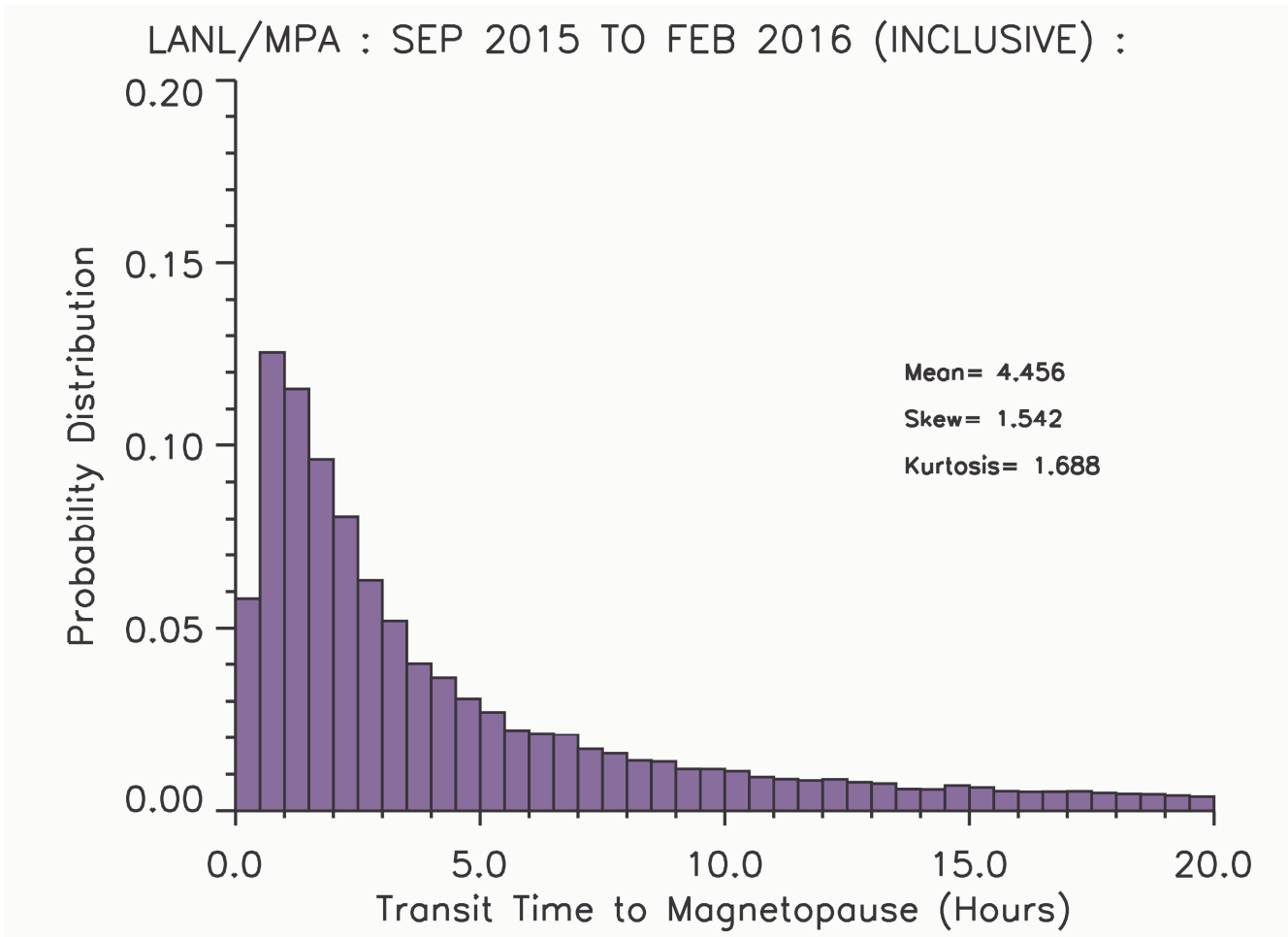
Figure 3. Scatter plots of density (top panel) and flow speed (bottom panel) of all cold ions sampled by MPA between September 2015 and February 2016 as a function of MLT and Kp (magnetosheath intervals are excluded).



495
 496
 497
 498
 499
 500

Figure 4. Probability distributions plots of density and flow speed for calm intervals (left column : $K_p < 1^+$) and disturbed intervals (right column : $K_p > 3$). All available data Sept. 2015 to Feb 2016 are plotted for the magnetic local time region between 12 and 18 MLT.

501



502

503

504

505

506

Figure 5. The probability distribution of (minimum) transport times from GEO to the estimated magnetopause location based on the *Shue et al.* [1998] model. All available data from 12-18 MLT and $K_p > 3$ are plotted.